



The two-spin model of a tracking chamber: a phase-space perspective

Luigi Barletti¹

Received: 26 June 2021 / Accepted: 9 September 2021
© The Author(s) 2021

Abstract

We study the dynamics of classical localization in a simple, one-dimensional model of a tracking chamber. The emitted particle is represented by a superposition of Gaussian wave packets moving in opposite directions, and the detectors are two spins in fixed, opposite positions with respect to the central emitter. At variance with other similar studies, we give here a phase-space representation of the dynamics in terms of the Wigner matrix of the system. This allows a better visualization of the phenomenon and helps in its interpretation. In particular, we discuss the relationship of the localization process with the properties of entanglement possessed by the system.

Keywords Mott problem · Localization · Entanglement · Wigner function

1 Introduction

Since the early days of quantum physics, one of the fundamental questions has been how our “classical” world can emerge from its quantum mechanical substrate. A paradigmatic situation is represented by the so-called Mott problem [9]: an alpha-particle emitter in a cloud chamber generates a spherically symmetric wave function, which propagates in the chamber according to Schrödinger equation; yet the particle wave produces in the chamber a track corresponding to a classical trajectory (a radial, straight line originating from the emitter). Such apparently contradictory phenomenon is named “classical localization.”

In order to explain this phenomenon, Mott studied a model where a central emitter injects a spherical wave function (the particle) and the cloud chamber is represented by an environment made of only two atoms in fixed (but generic) positions. The detection of the particle at a certain position corresponds to the ionization of the atom that occupies that position. Mott showed that the probability of *both* atoms being ionized is nearly zero unless the two atoms are aligned with the emitter. The interpretation of this fact is that the particle manifests itself only along a radial trajectory.

This confirms, or at least indicates, that the phenomenon of classical localization emerges naturally from the laws of quantum mechanics.

Since then, the model has been refined in several ways [3–5, 10, 11]; see also Ref. [7] and references therein. In particular, a one-dimensional model with N spins at fixed positions on each side of a central emitter has been theoretically and numerically studied in Refs. [3, 4, 11]. In this case, the particle “spherical wave” is represented by the superposition of two wave packets moving in opposite directions, and the detection of the particle corresponds to the spin flip. These studies have confirmed and reinforced the original Mott’s result, to the extent that the configurations with the largest probability turn out to be those where the majority of spins have been flipped on just one side of the “chamber.” Because of the symmetry of the problem, the probability of such states is equally distributed at the two sides, which means that the side where the track is formed is completely random, in the same way as in the cloud chamber the tracks form towards any direction with equal probability.

In this paper, we consider an oversimplified one-dimensional model of this kind, with only two spins in symmetrical positions with respect to the central emitter. At variance with the standard setup, we adopt here a phase-space formulation [1, 2, 6, 8, 12] and follow the evolution of the (matrix-valued) Wigner function of the system. In spite of its simplicity, this model, together with the phase-space perspective, turns out to be rather useful to visualizing, and perhaps better understanding, the localization

✉ Luigi Barletti
luigi.barletti@unifi.it

¹ Dipartimento di Matematica e Informatica “Ulisse Dini”,
Università degli Studi di Firenze, Viale Morgagni 67/A,
50134 Firenze, Italy

dynamics and its relationships with entanglement. In particular, we will show that localization is tightly related to the initial independence of particle and spins, and to the properties of “local” entanglement of the system.

The paper is organized as follows. In Sect. 2, we establish the mathematical formulation of the model in terms of the system wave function. In Sect. 3, the model is translated into the spinorial Pauli–Wigner formalism. Section 4 is devoted to the numerical experiments and their interpretation. The conclusions are drawn in Sect. 5.

2 The model

Let us consider an oversimplified model of a one-dimensional tracking chamber consisting of a particle emitter, placed at $x = 0$, and of two $\frac{1}{2}$ -spins, acting as detectors, that are placed at fixed positions $-r$ and r at the two sides of the emitter. The particle interacts with the spins, and it is “detected” when the spin along a given direction, say z , is flipped.

A particle-detectors quantum state is therefore described by a wave function $\Psi(x)$ belonging to the space

$$L^2(\mathbb{R}, \mathbb{C}) \otimes \mathbb{C}^2 \otimes \mathbb{C}^2 \equiv L^2(\mathbb{R}, \mathbb{C}^4).$$

Hence, Ψ is a 4-component spinor of the following form

$$\Psi(x) = \begin{pmatrix} \Psi_{uu}(x) \\ \Psi_{ud}(x) \\ \Psi_{du}(x) \\ \Psi_{dd}(x) \end{pmatrix}, \quad (1)$$

where $\Psi_{\sigma\tau}(x)$ is the wave function of the system with the left spin up ($\sigma = u$) or down ($\sigma = d$), and right spin up ($\tau = u$) or down ($\tau = d$). Then, for example, $|\Psi_{du}(x)|^2$ can be interpreted as the probability density that the particle is in position x , the left spin is down, and the right spin is up.

The dynamics of the system is assumed to be described (in suitably non-dimensionalized variables) by the Schrödinger equation

$$i\partial_t \Psi = H\Psi \quad (2)$$

where

$$H = -\frac{1}{2}\partial_{xx} \sigma_0 \otimes \sigma_0 + \gamma_{-r}(x)\sigma_1 \otimes \sigma_0 + \gamma_{+r}(x)\sigma_0 \otimes \sigma_1 \quad (3)$$

is the Hamiltonian. Here, $\gamma_{\pm r}(x) = \gamma(x \mp r)$, where $\gamma(x)$ is a real function localized around $x = 0$ (e.g., a Gaussian-shaped function), and

$$\sigma_0 = \begin{pmatrix} 1 & 0 \\ 0 & 1 \end{pmatrix}, \quad \sigma_1 = \begin{pmatrix} 0 & 1 \\ 1 & 0 \end{pmatrix}, \quad \sigma_2 = \begin{pmatrix} 0 & -i \\ i & 0 \end{pmatrix},$$

$$\sigma_3 = \begin{pmatrix} 1 & 0 \\ 0 & -1 \end{pmatrix}$$

are the Pauli matrices. Note that $\sigma_0 \otimes \sigma_0$ is the 4×4 identity matrix and

$$\sigma_1 \otimes \sigma_0 = \begin{pmatrix} 0 & \sigma_0 \\ \sigma_0 & 0 \end{pmatrix}, \quad \sigma_0 \otimes \sigma_1 = \begin{pmatrix} \sigma_1 & 0 \\ 0 & \sigma_1 \end{pmatrix}.$$

In the Hamiltonian (3), the interaction of the first spin is localized around $x = -r$, and the interaction of the second spin is localized around $x = r$ (this is indeed what allows us to speak of “left” and “right” spin). Since in both cases the interaction is proportional to σ_1 , it has the form of the interaction with a “magnetic field” oriented in the x -direction.

The model is completed by a suitable choice of the initial datum. Since in the actual cloud chamber the particle wave function is a spherical wave originating from the emitter, in the corresponding one-dimensional picture we consider a symmetrical wave function consisting of two Gaussian packets moving in opposite directions (representing therefore a “one-dimensional spherical wave”). We moreover assume that both spins are initially in the “up” state. This picture corresponds to an initial datum of the form

$$\Psi(x, 0) = \frac{\cos(k_0 x) e^{-x^2/4\delta^2}}{\sqrt[4]{2\pi\delta^2} e^{-k_0^2\delta^2/2} \sqrt{\cosh(k_0^2\delta^2)}} \begin{pmatrix} 1 \\ 0 \\ 0 \\ 0 \end{pmatrix}. \quad (4)$$

This is a superposition of two Gaussian wave packets, initially centered at $x = 0$, with position variance δ^2 , moving away from the origin with velocities $-k_0$ and $+k_0$, respectively. The fact that only the first component Ψ_{uu} of the spinor is nonzero means that in such initial state both spins are up. The spinor $\Psi(x, 0)$ is normalized to unity in the norm of $L^2(\mathbb{R}, \mathbb{C}^4)$, that is

$$\|\Psi\|^2 := \|\Psi_{uu}\|^2 + \|\Psi_{ud}\|^2 + \|\Psi_{du}\|^2 + \|\Psi_{dd}\|^2 = 1. \quad (5)$$

Now, the dynamics of the system can be intuitively described as follows. Initially, the two packets move away from the origin and the two spins remain up. As soon as the packets touch the zones where $\gamma_{\pm r}$ are significantly different from zero, the interactions are triggered and the three components Ψ_{ud} , Ψ_{du} , Ψ_{dd} , begin to populate, which means that the spins will get a certain probability to be found in the ud , du and dd states. In the same time, the two wave packets are scattered (partially reflected, partially transmitted) by the interaction. Incidentally, the presence of reflected waves that undergo significant multiple interactions is the main difference that the one-dimensional case has got with respect to the two-

three-dimensional ones, where the importance of multiple interactions of scattered waves is much less [11]. However, this fact will not qualitatively affect our conclusions since, as we will see, they can be drawn *before* the reflected wave reach again the spins. When the interactions are over, the different spin states stabilize to certain probabilities: $\|\Psi_{uu}\|^2$ is the probability that both spin are up (the particle has not been detected) $\|\Psi_{ud}\|^2$ is the probability that only the right spin is down (the particle has been detected on the right-hand side), $\|\Psi_{du}\|^2$ is the probability that only the left spin is down (the particle has been detected on the left-hand side), $\|\Psi_{dd}\|^2$ is the probability that both spins are down (the particle has been detected on both sides). The fact that the Schrödinger evolution (2) is unitary guarantees that the four probabilities sum up to one, as it was for the initial state.

Remarkably, it turns out that the final probability $\|\Psi_{dd}\|^2$ is nearly zero, which means that the particle is either not detected at all or it is only detected on one side. This is the one-dimensional analogue of the formation of a classical track from a spherical quantum wave, i.e., the phenomenon pointed out by Mott.

Numerical experiments with N spins (corresponding to a spinor with 2^N components) have confirmed the fact that the track formation (i.e., detection on one side) is more and more pronounced as N grows, giving a numerical evidence of the transition from quantum to classical behaviour [3, 5, 7, 10]. Current numerical experiments are able to consider up to $N = 14$ [4] and are all performed in the one-dimensional case.

In the next sections, we will try to look more closely at the dynamics of the system. We will use the Wigner representation to have a more intuitive visualization, and we will try to better understand why the probability of detection at both sides is so small.

3 The Wigner picture

3.1 The Wigner function of a two-spin system

In what follows, we will exploit the algebra of Pauli matrices and so let us recall some basic facts about it. The Pauli matrices σ_k , $k = 0, 1, 2, 3$ (we recall that σ_0 is the identity matrix) have the product rule

$$\sigma_i \sigma_j = \delta_{ij} \sigma_0 + i \epsilon_{ijk} \sigma_k, \tag{6}$$

for $1 \leq i, j, k \leq 3$, where δ_{ij} is the Kronecker symbol and ϵ_{ijk} is the Levi-Civita symbol. It follows that the four matrices

$$S_k = \frac{1}{2} \sigma_k, \quad k = 0, 1, 2, 3 \tag{7}$$

form an orthonormal basis of the space $\mathbb{C}^{2,2}$, of 2×2 complex matrices, with respect to the Hermitian product

$$\text{tr}(a^\dagger b), \tag{8}$$

where $a, b \in \mathbb{C}^{2,2}$, tr denotes the matrix trace and a^\dagger is a transposed and conjugated. Then, any $a \in \mathbb{C}^{2,2}$ can be uniquely decomposed as

$$a = \sum_{k=0}^3 a_k S_k, \quad a_k = \text{tr}(S_k a), \quad k = 0, 1, 2, 3. \tag{9}$$

(note that $S_k^\dagger = S_k$). We will refer to a_0, a_1, a_2, a_3 as the Pauli components of a . It is easily shown that the Pauli components are real if and only if $a = a^\dagger$, i.e., if a is Hermitian.

In the quantum mechanics of a single spin, the three matrices S_1, S_2 and S_3 represent the spin in the directions x , y and z , respectively. Then, if $\rho \in \mathbb{C}^{2,2}$ is the density matrix of a single-spin system (with no other degree of freedom than the spin itself), the expected value of the spin in the three directions is given by

$$\text{tr}(S_k \rho) = \rho_k, \quad k = 1, 2, 3,$$

which provides a direct physical interpretation of the Pauli components of ρ .

For a system of two spins (and no other degree of freedom), the state space is $\mathbb{C}^2 \otimes \mathbb{C}^2$, which can be identified with \mathbb{C}^4 , and the observables and the density matrices are 4×4 , Hermitian complex matrices. A basis of the space $\mathbb{C}^{4,4}$ of 4×4 complex matrices can be constructed by taking all tensor products of the Pauli matrices

$$S_{ij} = S_i \otimes S_j = \frac{1}{4} \sigma_i \otimes \sigma_j \quad 0 \leq i, j \leq 3. \tag{10}$$

The sixteen matrices S_{ij} constitute an orthonormal basis with respect to the Hermitian product (8) (where now $a, b \in \mathbb{C}^{4,4}$). Therefore, every $a \in \mathbb{C}^{4,4}$ is uniquely decomposed as

$$a = \sum_{i,j=0}^3 a_{ij} S_{ij}, \quad a_{ij} = \text{tr}(S_{ij} a) \tag{11}$$

and the components a_{ij} will be real when $a^\dagger = a$. In particular, if $\rho \in \mathbb{C}^{4,4}$ is the density matrix of a two-spin system, the components of the type

$$\rho_{i0} = \text{tr}(S_{i0} \rho) \quad \text{and} \quad \rho_{0j} = \text{tr}(S_{0j} \rho),$$

with $1 \leq i, j \leq 3$, have, respectively, the physical meaning of the expected value of the spin in the i th direction and of the second spin in the j th direction. A component of the type

$$\rho_{ij} = \text{tr}(S_{ij} \rho),$$

with $1 \leq i, j \leq 3$ is the expected value of the product of the i th component of the first spin with the j th component of

the second spin (it is therefore a spin correlation). It is also important to remark that the first row $(\rho_{00}, \rho_{10}, \rho_{20}, \rho_{30})$ and the first column $(\rho_{00}, \rho_{01}, \rho_{02}, \rho_{03})^T$ of the matrix ρ_{ij} contain the components of the reduced density matrices relative to, respectively, the first and the second spin.

We now consider also the continuous degree of freedom and work in the state space $L^2(\mathbb{R}, \mathbb{C}^4)$. The density matrix associated with the state (1) is the $\mathbb{C}^{4,4}$ -valued function

$$\rho(x, y) = \Psi(x) \otimes \Psi^*(y), \quad x, y \in \mathbb{R},$$

(Ψ^* denoting the complex conjugate of Ψ) and the corresponding $\mathbb{C}^{4,4}$ -valued Wigner function (Wigner matrix) is

$$W(x, p) = \int \rho(x + \xi/2, x - \xi/2) e^{-i\xi p} d\xi, \quad x, p \in \mathbb{R}. \tag{12}$$

The Hermitian symmetry of ρ , i.e., $\rho(x, y) = \rho^\dagger(y, x)$, implies that $W(x, p) = W^\dagger(x, p)$, i.e., W is a pointwise Hermitian matrix. Hence, the sixteen Pauli components of W ,

$$w_{ij}(x, p) = \text{tr}(S_{ij}W(x, p)), \tag{13}$$

are real-valued functions on phase space.

It is readily seen that the projections on single-spin up/down states are

$$P_\pm = S_0 \pm S_3$$

and the projection on the two-spin up/down states are

$$\begin{aligned} P_{\epsilon_1, \epsilon_2} &= P_{\epsilon_1} \otimes P_{\epsilon_2} \\ &= S_{00} + \epsilon_1 S_{30} + \epsilon_2 S_{03} + \epsilon_1 \epsilon_2 S_{33}, \end{aligned} \tag{14}$$

for $\epsilon_1, \epsilon_2 \in \{+, -\}$ (where $+$ corresponds to up and $-$ to down). The probability densities of the two-spin up/down states can be therefore retrieved from W in the following way:

$$\begin{aligned} |\Psi_{uu}(x)|^2 &= \int (w_{00} + w_{30} + w_{03} + w_{33})(x, p) dp, \\ |\Psi_{ud}(x)|^2 &= \int (w_{00} + w_{30} - w_{03} - w_{33})(x, p) dp, \\ |\Psi_{du}(x)|^2 &= \int (w_{00} - w_{30} + w_{03} - w_{33})(x, p) dp, \\ |\Psi_{dd}(x)|^2 &= \int (w_{00} - w_{30} - w_{03} + w_{33})(x, p) dp. \end{aligned} \tag{15}$$

Let us end this section by giving some bibliography where the interested reader can find a deeper introduction to the concepts that have been briefly exposed here. General references for the Wigner formalism in quantum mechanics are (among many others) Refs. [1, 6, 8, 12]. A reference for the spinorial Wigner function is, e.g., Ref. [2]: although only the

case of a single spin is considered there, the case of multiple spins is a straightforward generalization.

3.2 Dynamics of the wigner function

The evolution equation for W can be straightforwardly obtained from the Schrödinger equation (2)–(3). Indeed, the equation for $\rho(x, y, t) = \Psi(x, t) \otimes \Psi^*(y, t)$ (the von Neumann equation) reads as follows:

$$\begin{aligned} i\partial_t \rho(x, y, t) &= (H\Psi)(x, t) \otimes \\ &\Psi^*(y, t) - \Psi(x, t) \otimes (H\Psi)^*(y, t), \end{aligned}$$

so that (recalling (10))

$$\begin{aligned} i\partial_t \rho &= -\frac{1}{2}(\partial_{xx} - \partial_{yy})\rho + 4[\gamma_{-r}(x)S_{10}\rho - \gamma_{-r}(y)\rho S_{10}] \\ &+ 4[\gamma_{+r}(x)S_{01}\rho - \gamma_{+r}(y)\rho S_{01}]. \end{aligned} \tag{16}$$

By taking the Wigner transform of both sides [1, 2], we deduce the evolution equation for $W(x, p, t)$:

$$\begin{aligned} \partial_t W &= -p\partial_x W - 4i\left[\gamma_{-r}\left(x + \frac{1}{2}i\partial_p\right)S_{10}W \right. \\ &\quad \left. - \gamma_{-r}\left(x - \frac{1}{2}i\partial_p\right)WS_{10}\right] \\ &\quad - 4i\left[\gamma_{+r}\left(x + \frac{1}{2}i\partial_p\right)S_{01}W \right. \\ &\quad \left. - \gamma_{+r}\left(x - \frac{1}{2}i\partial_p\right)WS_{01}\right], \end{aligned} \tag{17}$$

where we used the standard notation for the pseudo-differential operators

$$f(i\partial_p)W(p) \equiv \frac{1}{2\pi} \int f(\xi)W(p')e^{-i(p-p')\xi} d\xi dp'.$$

The initial Wigner matrix is the Wigner transform of $\Psi(x, 0) \otimes \Psi^*(y, 0)$, where $\Psi(x, 0)$ is given by (4). This can be explicitly computed and yields (in terms of the matrix of Pauli components)

$$W(x, p, 0) = w_0(x, p) \begin{pmatrix} 1 & 0 & 0 & 1 \\ 0 & 0 & 0 & 0 \\ 0 & 0 & 0 & 0 \\ 1 & 0 & 0 & 1 \end{pmatrix}, \tag{18}$$

where

$$\begin{aligned} w_0(x, p) &= N e^{-\frac{1}{2\delta^2}x^2} \left[e^{-2\delta^2(p+k_0)^2} \right. \\ &\quad \left. + e^{-2\delta^2(p-k_0)^2} + e^{-2\delta^2 p^2} \cos(2k_0 x) \right], \end{aligned} \tag{19}$$

the normalization constant being

$$N = \frac{1}{8\pi e^{-k_0^2 \delta^2} \cosh(k_0^2 \delta^2)}.$$

Note that the Wigner function $w_0(x, p)$ is the sum of three terms. The first two terms are “classical” Maxwellians centered at $(x = 0, p = -k_0)$ and $(x = 0, p = +k_0)$, respectively, hence with opposite mean velocities (remember that, in our nondimensional variables, k_0 is at the same time a wave-number, a momentum and a velocity). The third term is a Maxwellian centered at $(x = 0, p = 0)$, which modulates the oscillation $\cos(2k_0 x)$; this is interpreted as the quantum interference fringes between the two counter-moving wave packets. Note also that the momentum variance is $1/4\delta^2$, which reflects the minimal indetermination relation of a Gaussian state. The function (19) is a well known, and somehow prototypical, example of Wigner function (see, e.g., the cover of the book [12]). Here, we interpret w_0 as the Wigner function of the “one-dimensional spherical wave” produced by the emitter.

We finally remark that in (18) the only nonzero Pauli components of the initial W are $w_{00}, w_{30}, w_{03}, w_{33}$. This corresponds to the fact that, at the initial time, the two spins are both in the up state and are completely uncorrelated (they are in a product state).

4 Numerical experiments

4.1 Simulation setting

For the numerical experiments, we consider a phase-space domain $x \in [-20, 20]$, $p \in [-10, 10]$, and a time domain $T \in [0, 3]$ (recall that we are working in nondimensional variables). The initial position spread is assumed to be $\delta = 0.8$ and the “spherical wave velocity” is assumed to be $k_0 = 4$. The two spins are placed at $x = \pm r$, with $r = 7$, and the interaction function γ is assumed to have the super-Gaussian shape

$$\gamma(x) = \alpha e^{-x^4/2\lambda^2}, \quad (20)$$

with $\alpha = 2$ and $\lambda = 0.4$. The above values are chosen so that:

1. the wave has enough time to interact with the two spins and then move away;
2. within the simulation time, the wave has no significant overlap with the border of the computational domain;
3. the reflected waves are small and have not enough time to re-interact with the opposite spin.

Condition 2 implies that the experiments we perform are insensitive to the chosen boundary conditions (incidentally, we impose non re-entry conditions). Condition

3 is very important, since multiple interactions of the reflected waves represent a limitation of the one-dimensional model with respect to the realistic three-dimensional situation, where reflected waves play a negligible role [11].

For the numerical implementation of Eq. (17) we use a simple splitting scheme. Each time step Δt is divided into two substeps of length $\Delta t/2$: In the first one, only the free-transport operator $-p\partial_x$ is considered and the system evolves according to

$$W(x, p, t + \Delta t/2) = W(x - p\Delta t/2, p, t).$$

In the second one, only the interaction (second and third terms at the right-hand side of Eq. (17)) operates between $t + \Delta t/2$ and $t + \Delta t$. Since a pseudo-differential operator is involved, this interaction step is easily implemented by using back and forth Fourier transform. We remark that the present paper is focused on the model and not on the numerical aspects: we just chose a simple numerical method, which is certainly not the most efficient nor the most accurate one.

4.2 Dynamics of localization

In Figs. 1 and 2, we can follow the evolution of some of the Pauli components of the Wigner matrix $W(x, p, t)$.

In particular, Fig. 1 displays w_{00}, w_{30}, w_{03} and w_{33} , which are the only initially non-zero components (see (18)) and which determine the probabilities of the up/down states, according to (15). Each column contains a time snapshot of the four components in the phase space (x, p) . Here and in the following figures, the background gray corresponds to the value 0, the lighter gray corresponds to positive values and the darker gray to negative ones. At $t = 0$ we can see therefore the gray-level representation of $w_0(x, p)$: note the two counter-moving Gaussians and the central interference fringes. The two Gaussians move freely until they reach the two spins (concentrated around $x = \pm 7$) and the interaction begins, turning the spin from up (positive values) to down (negative values). Once the interaction zones have been overcome, the transmitted waves move away freely. Note also the presence of small reflected waves (the reflected portion of the wave is larger when the interaction strength α is increased).

To interpret these pictures, let us recall that w_{00} is the Wigner function of the system where the spin degrees of freedom are traced out; hence w_{00} is the pseudo-distribution in phase space of the emitted particle. Analogously, w_{30} (respectively, w_{03}) can be interpreted as the pseudo-distribution in phase space of the value of the z -component of the left (respectively, right) spin. Note that, after the interaction, the state of the *left* spin is down on the left-hand side and up on the right-hand side. This corresponds to the fact that

Fig. 1 Grayscale plots showing the evolution of the components w_{00} , w_{30} , w_{03} and w_{33} of the Wigner matrix. The background gray corresponds to 0, the lighter gray to positive values and the darker gray to negative ones

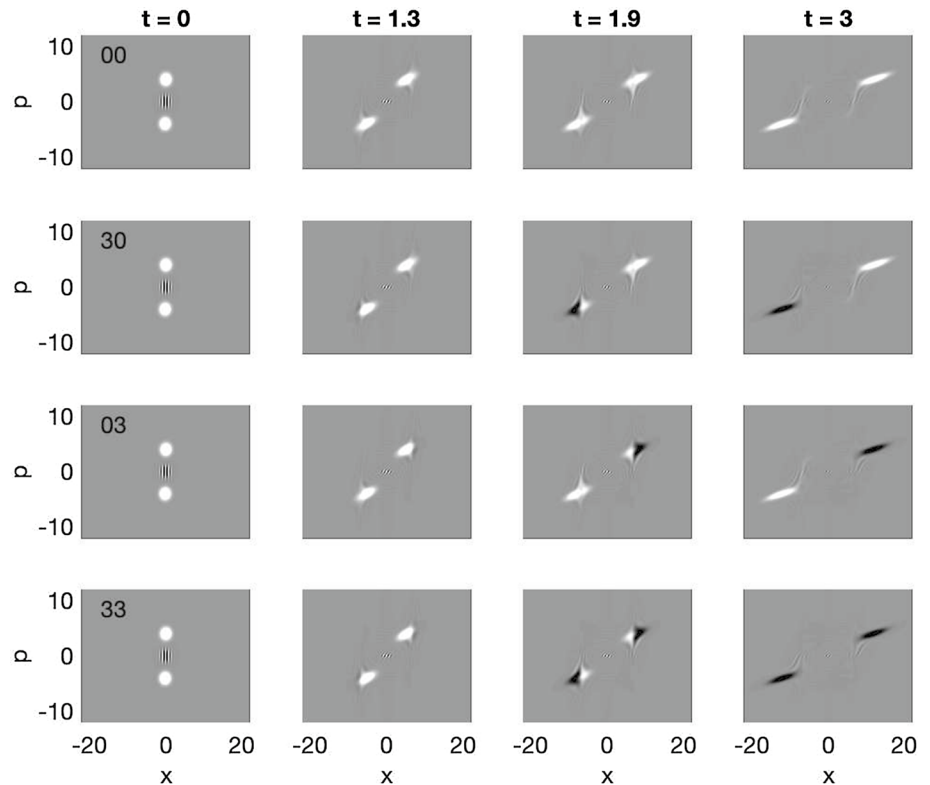
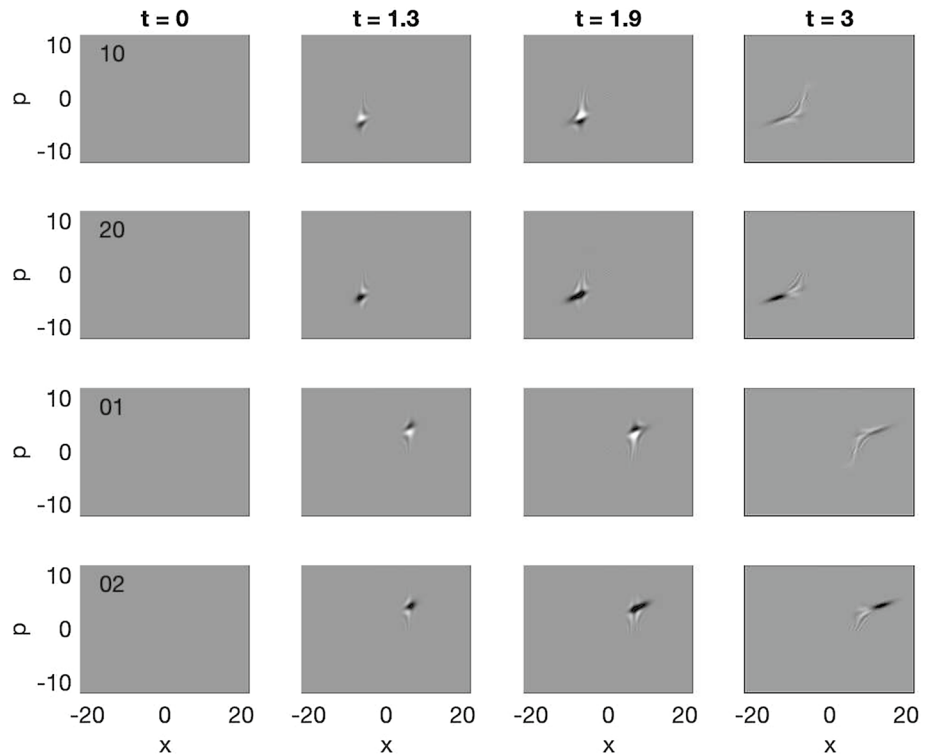


Fig. 2 Same as Fig. 1 but for the components w_{10} , w_{20} , w_{01} and w_{02} (the x - and y -components of each spin). They are initially zero and acquire nonzero values with the interaction. In a semiclassical perspective, the spin vector rotates around the “magnetic field” $\gamma_{\pm r} \sigma_1$ (which is oriented in the x -direction), and therefore, the x -component of the spin should remain equal to 0 at any time. In the quantum evolution, this is only true “on average”: by computing the integrals of w_{10} and w_{01} with respect to p one obtains 0 (in the pictures, we can note the oscillations that produce such null average)



the left spin is down if the particle will be detected on the left and it is up if the particle will be detected on the right (of course, the symmetrical conclusions can be drawn on

the right spin). Therefore, the component w_{33} , which is the pseudo-distribution of the product of the z -component of the two spins, is always negative after the interaction.

Figure 2 shows the evolution of other spin components: Since they are not directly involved in the localization process, we shall limit ourselves to commenting on them briefly in the figure caption.

Let us rather look at Fig. 3, where we plot the Wigner functions

$$\begin{aligned}
 w_{uu} &= w_{00} + w_{30} + w_{03} + w_{33}, \\
 w_{ud} &= w_{00} + w_{30} - w_{03} - w_{33}, \\
 w_{du} &= w_{00} - w_{30} + w_{03} - w_{33}, \\
 w_{dd} &= w_{00} - w_{30} - w_{03} + w_{33},
 \end{aligned}
 \tag{21}$$

which, according to (15), can be interpreted as the phase-space quasi-distributions of the uu , ud , du and dd states. It is immediately apparent that at $t = 0$ only the uu state is populated while, after the interactions, the ud and du states gain the highest probability, and the dd state remains with zero probability. Indeed, computing the integrals over phase space of the four components at $t = 3$ yields the total probabilities

$$\begin{aligned}
 \|\Psi_{uu}\|^2 &= 0.1664, & \|\Psi_{ud}\|^2 &= 0.4168, & \|\Psi_{du}\|^2 &= 0.4168, \\
 \|\Psi_{dd}\|^2 &= 0.0000.
 \end{aligned}$$

As already mentioned in Sect. 2, such values are the sign of localization: the probability of detecting the particle at both sides is nearly zero, while the larger probability is that of detecting the particle on one of the two sides (with equal

probability). There is also a certain probability that the particle is not detected at all, which depends on the interaction strength α . We remark that there might be a tiny nonzero probability of detection at both sides, due to reflected waves (and to the non-perfect locality of the interaction function γ): as already pointed out, the effect of reflected waves is even smaller in the two- or three-dimensional cases.

By comparing Figs. 1 and 3, it is clear from (21) that the prevalence of w_{ud} and w_{du} , and the smallness of w_{dd} can be interpreted in terms of constructive/destructive interference among the components w_{00} , w_{30} , w_{03} and w_{33} . But a more insightful way to understand the phenomenon is in terms of projections and entanglement, which will be treated in the next subsection.

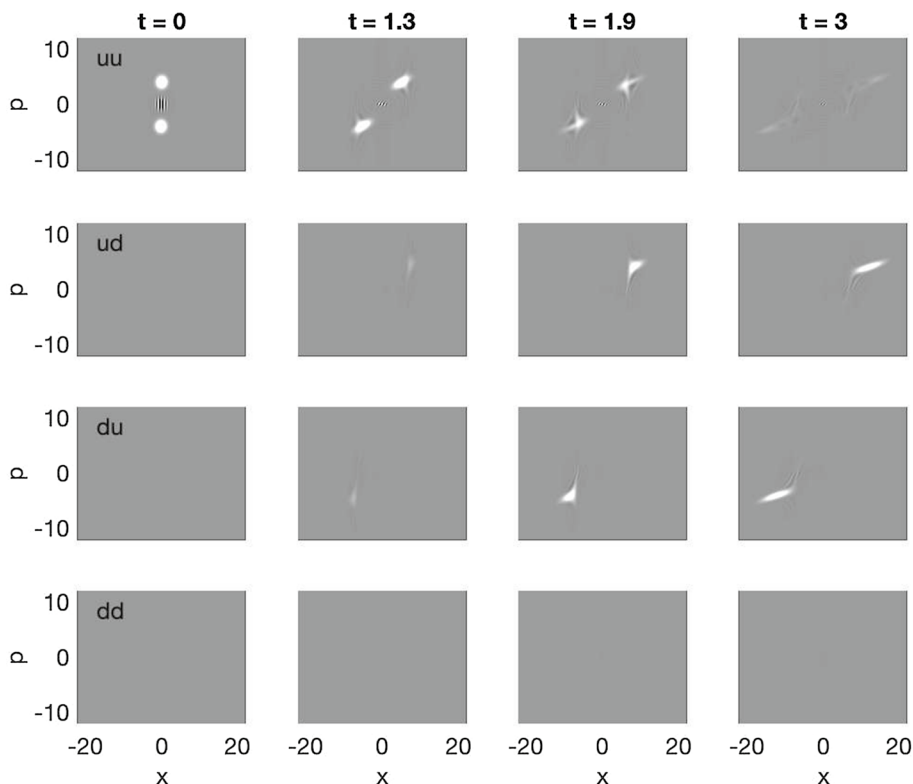
4.3 Relationships with entanglement

It will be useful to adopt Dirac’s notation for the spin states. Our initial state can be represented as

$$\psi|u\rangle|u\rangle$$

where ψ is the initial particle wave function, the first $|u\rangle$ is the initial state of the left spin and the second $|u\rangle$ is the initial state of the right spin (both are up). The fact that the state is factorized corresponds to the initial independence of the particle and the two spins. The initial particle wave function is the sum of the two wave packets with mean velocities $-k_0$

Fig. 3 Same as Fig. 1 but for the components w_{uu} , w_{ud} , w_{du} and w_{dd}



and $+k_0$. So, before the interaction, the state of the system keeps the form

$$\psi^-|u\rangle|u\rangle + \psi^+|u\rangle|u\rangle,$$

where ψ^\pm denote the two counter-moving wave packets as they have moved away from the origin (ψ^- and ψ^+ being approximately localized at $x < 0$ and $x > 0$, respectively). In this situation, the projections P_{ud} , P_{du} and P_{dd} (see Eq. (14), where the plus sign corresponds to u and the minus sign corresponds to d) are of course zero. In terms of the Wigner matrix, this situation can be visualized in the first column of Figs. 1, 2 and 3. Then, interactions take place (second and third columns of Figs. 1, 2 and 3), progressively increasing the d -component of the left and right spins. After that (fourth column of Figs. 1, 2 and 3), the state has (schematically) the form

$$(\psi_u^-|u\rangle + \psi_d^-|d\rangle)|u\rangle + |u\rangle(\psi_u^+|u\rangle + \psi_d^+|d\rangle), \quad (22)$$

where ψ_u^\pm and ψ_d^\pm are position-dependent coefficients. We see therefore that the state is not factorized any longer (indeed, it is an entangled state) but, nevertheless, it is *locally*, side-wise, factorized. This implies that the P_{dd} projection of this state is null:

$$\begin{aligned} P_{dd}[(\psi_u^-|u\rangle + \psi_d^-|d\rangle)|u\rangle \\ + |u\rangle(\psi_u^+|u\rangle + \psi_d^+|d\rangle)] \\ = P_d(\psi_u^-|u\rangle + \psi_d^-|d\rangle)P_d|u\rangle \\ + P_d|u\rangle P_d(\psi_u^+|u\rangle + \psi_d^+|d\rangle) = 0, \end{aligned} \quad (23)$$

which explains the smallness of the dd component. Actually, the expression (22) of the final state is just an approximation, because a possible entanglement of the right spin on the left side and of the left spin on the right side arises from reflected waves (and also, but this is of course a negligible effect, from the non-perfect locality of the interaction function (20)). However, our simulations show that such approximation is really good, at least for the chosen values of the parameters. This is illustrated in Fig. 7, which is explained below.

What emerges from the preceding discussion is that two main facts determine the localization process:

1. The two spins and the particle are initially independent;
2. The interactions produce on each side the local entanglement of one spin and preserve the independence of the other one.

In order to illustrate point 1, let us change our experiment by assuming that the two spins are initially entangled. In particular, let us assume that they initially are in the so-called *singlet* state

$$\frac{|u\rangle|d\rangle - |d\rangle|u\rangle}{\sqrt{2}},$$

corresponding to an initial Wigner matrix (expressed in terms of the Pauli components) of the form

$$W(x, p, 0) = w_0(x, p) \begin{pmatrix} 1 & 0 & 0 & 0 \\ 0 & -1 & 0 & 0 \\ 0 & 0 & -1 & 0 \\ 0 & 0 & 0 & -1 \end{pmatrix}. \quad (24)$$

Figures 4 and 5 are the equivalent of Figs. 1 and 3 where the initial Wigner function (18) has been substituted with (24).

We see that the situation is now completely different and localization does not occur. On the contrary, the dd state gains the highest probability. By integration on phase space, we indeed obtain the post-interaction probabilities

$$\begin{aligned} \|\Psi_{uu}\|^2 = 0.4168, \quad \|\Psi_{ud}\|^2 = 0.0832, \quad \|\Psi_{du}\|^2 = 0.0832, \\ \|\Psi_{dd}\|^2 = 0.4168. \end{aligned}$$

Coming to point 2, we can check the emergence of entanglement in the system by computing the *purity* of the spin states. As it follows from the discussion in Sect. 3,

$$\rho_k = \int w_{k0}(x, p) dp dx, \quad k = 0, 1, 2, 3$$

are the Pauli components of the reduced density matrix ρ_{red} of the left spin (i.e., the density matrix obtained by tracing out the degrees of freedom of the right spin and of the particle). The purity index is defined as

$$\text{tr}(\rho_{red}^2) = \frac{1}{2} \sum_{k=0}^3 \rho_k^2. \quad (25)$$

If the left spin remains independent, then its reduced density matrix is that of a pure state (characterized by $\rho_1^2 + \rho_2^2 + \rho_3^2 = \rho_0^2 = 1$), and the purity index is 1. If the spin gets entangled, its reduced density matrix is that of a mixed state (characterized by $\rho_1^2 + \rho_2^2 + \rho_3^2 < \rho_0^2 = 1$) and the purity lies between 1/2 and 1. Figure 6 shows the computed evolution in time of the purity index in three cases: the case of the initially independent spins (corresponding to the initial datum (18)), the case of the initially entangled spins (corresponding to the initial datum (24)) and, as a further check, the case of initially independent spins without interaction (corresponding to initial datum (18) and $\alpha = 0$). As we can see from the figure, the interaction introduces entanglement in the initially unentangled system.

Let us address the local behaviour of the purity for initially independent spins. In Fig. 7, we plot four time snapshots of the x -dependent quantity

Fig. 4 Evolution of w_{00} , w_{30} , w_{03} and w_{33} in the case of singlet initial state

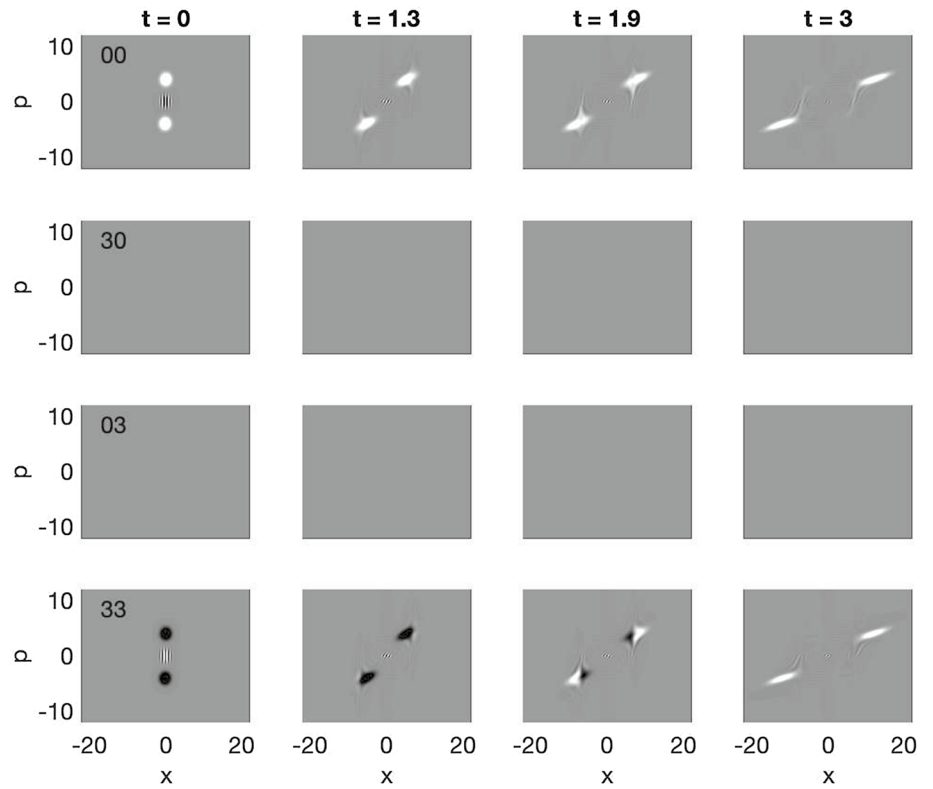
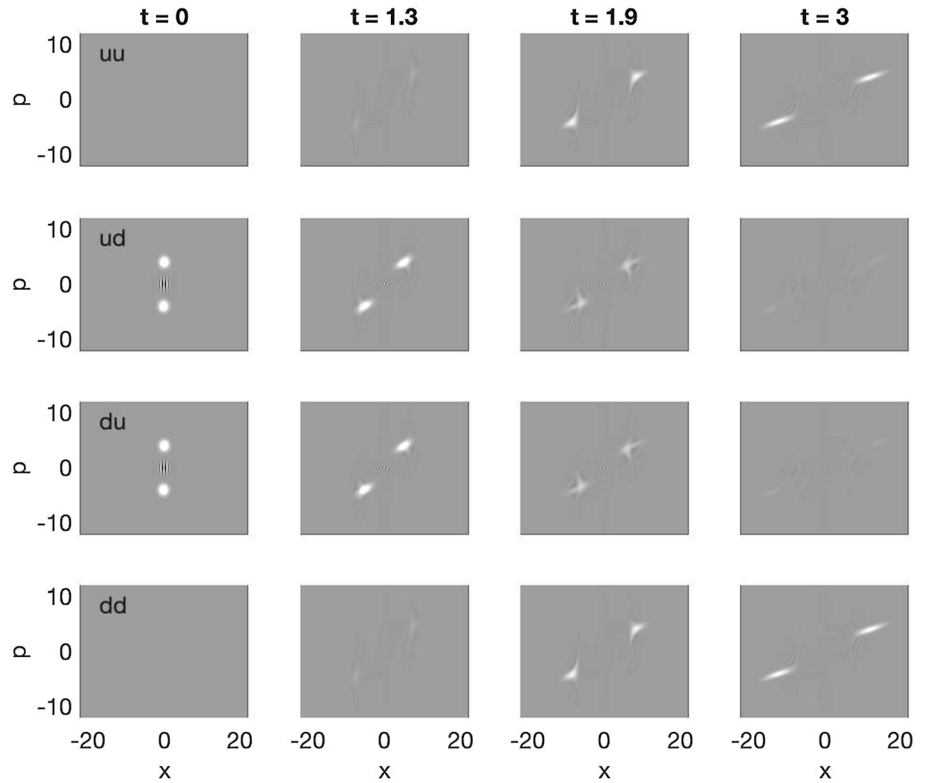


Fig. 5 Evolution of w_{uu} , w_{ud} , w_{du} and w_{dd} in the case of singlet initial state



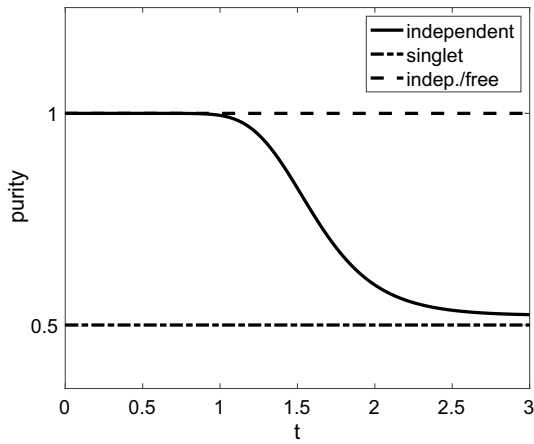


Fig. 6 Evolution of the left-spin purity (25) in three different cases. Continuous line: initially independent spins; dot-dashed line: initially entangled spins (singlet state); dashed line: initially independent spins with free evolution (obtained by setting $\alpha = 0$)

$$\left(\int w_{00}(x, p) dp \right)^2 - \sum_{k=1}^3 \left(\int w_{k0}(x, p) dp \right)^2, \quad (26)$$

which can be interpreted as a “local impurity” index of the left spin (it is zero if the reduced density matrix obtained by tracing out the right spin at fixed x is that of a pure state). We see that the left spin gets locally entangled (with

the particle) at the right-hand side while remaining locally independent on the right-hand side. Of course, the converse is true for the right spin. Figures 6 and 7 confirm the fact that interactions produce on each side local entanglement of one of the two spin, preserving the local independence of the other one, thus creating the conditions under which (23) holds and, therefore, localization takes place.

As a final remark, let us point out that if we had sent from the emitter *two* independent particles in the two directions, instead of the *single* particle we have sent, system entanglement and localization would have not occurred. In fact, for an initial state of the form

$$\psi \varphi |u\rangle|u\rangle$$

where now ψ is the wave function of a left-moving particle and φ is the wave function of another, right-moving, particle, the post-interaction state would have the form

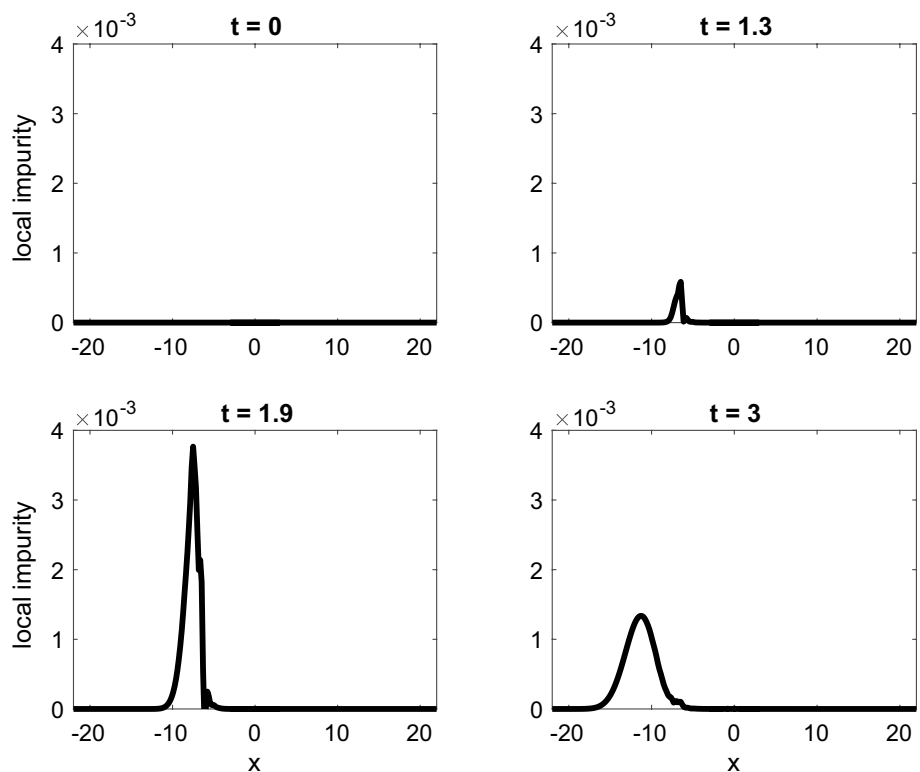
$$(\psi_u|u\rangle + \psi_d|d\rangle)(\varphi_u|u\rangle + \varphi_d|d\rangle),$$

since each spin has interacted with a different particle. In this case, the post-interaction dd state is given by

$$P_{dd}[(\psi_u|u\rangle + \psi_d|d\rangle)(\varphi_u|u\rangle + \varphi_d|d\rangle)] = P_d(\psi_u|u\rangle + \psi_d|d\rangle)P_d(\varphi_u|u\rangle + \varphi_d|d\rangle) = \psi_d|d\rangle + \varphi_d|d\rangle,$$

which has a nonzero amount of probability, depending on the efficiency of the spin flip. Indeed, the probability of

Fig. 7 Evolution of the “local impurity” of the left spin, defined by (26), in the case of the initially independent spins. We see that the left spin remains independent on the right



detecting *two* particles, one on each side, has no reason to be zero.

5 Conclusions

In this work, we have studied a very simple Mott-like model in the framework of the phase-space formulation of quantum mechanics. The heavier formalism required by this approach (sixteen real components of the Wigner matrix against the four complex components of the wave function) is compensated by two main advantages. The first one is a better visualization of the localization dynamics, in terms of “classical-looking” quasi-distributions in phase space. The second one is the fact that the reduced density matrices of the various subsystems are easily retrieved from the Wigner matrix, which allows a straightforward analysis of both global and local entanglement.

The numerical simulations, of course, confirm what is already well known, i.e., the fact that detection of the particle at both sides has probability close to zero, which, in the one-dimensional model, corresponds to classical localization. By means of simple considerations, we have shown that the main properties that lead to localization are the initial independence, the emergence of entanglement of the spins with the particle and the local (namely, side-wise) preservation of independence of the spin which is not interacting. The numerical simulations confirm such interpretation. Indeed, by repeating the experiment with the two spins in an initially entangled state, we observe that localization does not occur and detection at both sides gain the highest probability. Moreover, computing the purity and the “local impurity” (in the case of initial independence) confirms the dynamical onset of entanglement of just one spin per side.

It is clear that the same kind of considerations apply to the case of arrays of N spins ($N/2$ on each side), thus extending their validity beyond the simple, yet insightful, two-spin model considered in this work.

Acknowledgements The author acknowledges support from INdAM-GNFM (Italian National Group for Mathematical Physics).

Funding Open access funding provided by Università degli Studi di Firenze within the CRUI-CARE Agreement.

Availability of data and codes The codes and datasets generated during the current study are available from the author on reasonable request.

Declarations

Conflicts of interest. The author declares that he has no conflict of interest.

Open Access This article is licensed under a Creative Commons Attribution 4.0 International License, which permits use, sharing, adaptation, distribution and reproduction in any medium or format, as long as you give appropriate credit to the original author(s) and the source, provide a link to the Creative Commons licence, and indicate if changes were made. The images or other third party material in this article are included in the article's Creative Commons licence, unless indicated otherwise in a credit line to the material. If material is not included in the article's Creative Commons licence and your intended use is not permitted by statutory regulation or exceeds the permitted use, you will need to obtain permission directly from the copyright holder. To view a copy of this licence, visit <http://creativecommons.org/licenses/by/4.0/>.

References

1. Barletti, L.: A mathematical introduction to the Wigner formulation of quantum mechanics. *Boll. UMI* **6B**, 693–716 (2003)
2. Barletti, L., Frosali, G., Morandi, O.: Kinetic and hydrodynamic models for multi-band quantum transport in crystals. In: Ehrhardt, N., Koprucki, T. (eds.) *Multi-band effective mass approximations: advanced mathematical models and numerical techniques*, pp. 3–56. Springer, Berlin (2014)
3. Cacciapuoti, C., Carlone, R., Figari, R.: A solvable model of a tracking chamber. *Rep. Math. Phys.* **59**, 337–349 (2007)
4. Carlone, R., Figari, R., Negulescu, C.: A model of a quantum particle in a quantum environment: a numerical study. *Commun. Comput. Phys.* **18**, 247–262 (2015)
5. Dell’Antonio, G.F.: On tracks in a cloud chamber. *Found. Phys.* **45**, 11–21 (2015)
6. Ferry, D., Nedjalkov, M.: *The Wigner function in science and technology*. IOP Publishing, Bristol (2018)
7. Figari, R., Teta, A.: *Quantum dynamics of a particle in a tracking chamber*. Springer, Berlin (2014)
8. Folland, G.B.: *Harmonic analysis in phase space*. Princeton University Press, Princeton (1989)
9. Mott, N.F.: The wave mechanics of α -ray tracks. *Proc. R. Soc. Lond. A* **126**, 79–84 (1929)
10. Recchia, C., Teta, A.: Semiclassical wave-packets emerging from interaction with an environment. *J. Math. Phys.* **55**, 012104 (2014)
11. Sparenberg, J.-M., Gaspard, D.: Decoherence and determinism in a one-dimensional cloud-chamber model. *Found. Phys.* **48**, 429–439 (2018)
12. Zachos, C.K., Fairlie, D.B., Curtright, T.L. (eds.): *Quantum mechanics in phase space. An overview with selected papers*. World Scientific, Hackensack (2005)

Publisher's Note Springer Nature remains neutral with regard to jurisdictional claims in published maps and institutional affiliations.